Gene Expression, Vol. 17, pp. 237–249
Printed in the USA.

1052-2166/17 $90.00 + .00
DOI: https://doi.org/10.3727/105221617X695195
E-ISSN 1555-3884
www.cognizantcommunication.com

tomm22 Knockdown-Mediated Hepatocyte Damages Elicit Both the Formation of Hybrid Hepatocytes and Biliary Conversion to Hepatocytes in Zebrafish Larvae

Jianchen Wu,*† Tae-Young Choi,*[1] and Donghun Shin*

*Department of Developmental Biology, McGowan Institute for Regenerative Medicine, Pittsburgh Liver Research Center, University of Pittsburgh, Pittsburgh, PA, USA
†Tsinghua University School of Medicine, Beijing, P.R. China

The liver has a highly regenerative capacity. In the normal liver, hepatocytes proliferate to restore lost liver mass. However, when hepatocyte proliferation is impaired, biliary epithelial cells (BECs) activate and contribute to hepatocytes. We previously reported in zebrafish that upon severe hepatocyte ablation, BECs extensively contribute to regenerated hepatocytes. It was also speculated that BEC-driven liver regeneration might occur in another zebrafish liver injury model in which temporary knockdown of the mitochondrial import gene *tomm22* by morpholino antisense oligonucleotides (MO) induces hepatocyte death. Given the importance of multiple BEC-driven liver regeneration models for better elucidating the mechanisms underlying innate liver regeneration in the diseased liver, we hypothesized that BECs would contribute to hepatocytes in *tomm22* MO-injected larvae. In this MO-based liver injury model, by tracing the lineage of BECs, we found that BECs significantly contributed to hepatocytes. Moreover, we found that surviving, preexisting hepatocytes become BEC–hepatocyte hybrid cells in *tomm22* MO-injected larvae. Intriguingly, both the inhibition of Wnt/β-catenin signaling and macrophage ablation suppressed the formation of the hybrid hepatocytes. This new liver injury model in which both hepatocytes and BECs contribute to regenerated hepatocytes will aid in better understanding the mechanisms of innate liver regeneration in the diseased liver.

Key words: Liver regeneration; Macrophage; Oval cells; Liver progenitor cells

INTRODUCTION

The liver is a crucial organ with a remarkable regenerative capacity. Even after removing two thirds of the liver mass, the liver can recover the lost mass and restore its function[1]. In this regeneration setting, hepatocytes proliferate to make more hepatocytes, thereby recovering the lost liver mass. However, when hepatocyte proliferation is impaired, biliary epithelial cells (BECs) contribute to hepatocytes[2,3]. Based on the source of regenerated hepatocytes, liver regeneration can be classified into either hepatocyte- or BEC-driven liver regeneration. In BEC-driven liver regeneration, BECs are first activated to form oval cells, also called ductular reactions, and then differentiate into hepatocytes. Multiple lineage-tracing studies in mice have shown that in diverse oval cell activation models, including 3,5-diethoxycarbonyl-1,4-dihydrocollidine (DDC), a choline-deficient ethionine-supplemented (CDE) diet, CCl_4 administration, and α-naphthyl-isothiocyanate (ANIT) diet, regenerated hepatocytes are derived only from preexisting hepatocytes[4–8], indicating the negligible contribution of BECs to hepatocytes. In contrast to these oval cell activation models, two severe liver injury models have recently been described in which BECs extensively give rise to hepatocytes: (1) a mouse model in which the E3 ubiquitin ligase gene *Mdm2* is inducibly deleted in hepatocytes[9] and (2) a zebrafish model in which hepatocytes are pharmacogenetically ablated[10–12]. In the mouse model, the *Mdm2* deletion completely blocks hepatocyte proliferation and induces p53-mediated hepatocyte senescence and death, which triggers oval cell activation and their differentiation into hepatocytes[9]. In the zebrafish model, the transgenic zebrafish lines that express bacterial nitroreductase (NTR) enzyme under the hepatocyte-specific *fabp10a* promoter allow for hepatocyte-specific ablation. The NTR enzyme converts a nontoxic drug, metronidazole (Mtz), into a cytotoxic

[1]Current affiliation: Department of Genetic Resources Research, National Marine Biodiversity Institute of Korea, Seocheon-gun, Chungcheongnam-do 33662, Republic of Korea.
Address correspondence to Donghun Shin, Department of Developmental Biology, McGowan Institute for Regenerative Medicine, Pittsburgh Liver Research Center, University of Pittsburgh, 3501 5th Avenue #5063, Pittsburgh, PA 15260, USA. Tel: 1-412-624-2144; Fax: 1-412-383-2211; E-mail: donghuns@pitt.edu

drug, resulting in the ablation of only NTR-expressing cells[13–16]. Upon severe hepatocyte ablation in zebrafish larvae, BECs extensively contribute to hepatocytes, thereby leading to a full liver recovery[10–12].

Given the correlation between oval cell numbers and disease severity in diseased human livers[17] and a recent report that BECs appear to contribute to hepatocytes in regressed human cirrhotic livers[18], it is important to understand the mechanisms underlying BEC-driven liver regeneration, which will provide insights into promoting innate liver regeneration in patients with advanced liver diseases. Although the zebrafish hepatocyte ablation and the mouse *Mdm2* deletion models will contribute to the elucidation of the mechanisms underlying BEC-driven liver regeneration, additional liver injury models for this type of liver regeneration should further contribute to such elucidation. In fact, diverse oval cell activation models collectively contribute to the current understanding of the oval cell activation process[19]. Here we report a novel liver injury model resulting from the temporary knockdown of *tomm22*, in which BECs contribute to hepatocytes.

The mitochondrial import gene *tomm22* zebrafish mutants exhibit hepatocyte-specific cell death, leading to the death of the animal[20]. Similarly, *tomm22* knockdown using the morpholino antisense oligonucleotide (MO) approach initially results in hepatocyte death, but later new hepatocytes form and the liver recovers, following the gradual depletion of the MOs. Based on biliary marker expression, it was speculated that in *tomm22* MO-injected larvae, BECs gave rise to the new hepatocytes; however, no lineage-tracing data were formulated to confirm this speculation[20]. Since hepatocyte death induces BEC-driven liver regeneration in the zebrafish hepatocyte ablation model[10–12] and the mouse hepatocyte-specific *Mdm2* deletion model[9], we hypothesized that BECs contributed to the hepatocytes in *tomm22* MO-injected larvae. To test this hypothesis, we performed lineage tracing experiments to unequivocally determine the origin of new hepatocytes in *tomm22* MO-injected larvae. Surprisingly, we found that both preexisting hepatocytes and BECs contributed to the new hepatocytes in *tomm22* MO-injected larvae. Moreover, using the *tomm22* MO-based liver regeneration model, we investigated the role of Wnt/β-catenin signaling and macrophages in liver regeneration.

MATERIALS AND METHODS

Zebrafish Strains

Experiments were performed with the approval of the Institutional Animal Care and Use Committee (IACUC) at the University of Pittsburgh. Embryos and adult fish were raised and maintained under standard lab conditions[21]. We used the following transgenic lines: *Tg(Tp1:H2B-mCherry)*^{s939}[22], *Tg(ubb:loxP-GFP-loxP-mCherry)*^{cz1701}[23], *Tg(Tp1:CreERT2)*^{s951}[24], *Tg(fabp10a:mAGFP-gmnn)*^{pt608}[25], *Tg(WRE:d2GFP)*^{kyu1}[26], *Tg(mpeg1:Gal4-VP16)*^{gl24}[27], *Tg(UAS:NTR-mCherry)*^{c264}[14], *Tg(fabp10a:CFP-NTR)*^{s931}[12], *Tg(fabp10a:GFP)*^{as3}[28], and *Tg(mpeg1:Dendra2)*^{uwm12}[29].

Morpholino Injection

tomm22 MO (5′-GAGAAAGCTCCTGGATCGTAGC CAT-3′)[20] was purchased from GeneTools (Philomath, OR, USA); 6 ng of *tomm22* MO was injected into embryos at the one-cell stage.

Cre/loxP-Mediated Lineage Tracing, Macrophage Ablation, and Wnt/β-Catenin Suppression

For lineage tracing experiments, *Tg(fabp10a:CFP-NTR);Tg(ubb:loxP-GFP-loxP-mCherry);Tg(Tp1:Cre ERT2)* larvae were treated with 10 μM 4-hydroxytamoxifen (4-OHT) from 48 to 84 h postfertilization (hpf) for 36 h to induce Cre-mediated recombination. For macrophage ablation experiments, *Tg(mpeg1:Gal4-VP16);Tg(UAS:NTR-mCherry)* larvae were treated with 10 mM Mtz from 4 to 6 or 7 days postfertilization (dpf). For Wnt/β-catenin suppression experiments, larvae were treated with 10 μM XAV939 from 4 to 6 or 7 dpf.

Whole-Mount In Situ Hybridization and Immunostaining

Whole-mount in situ hybridization was performed as previously described[30]. We used the following probes: *prox1a*, *foxa3*, *sepp1b*, *cp*, and *fabp10a*. Whole-mount immunostaining was performed as previously described[31], using the following antibodies: chicken polyclonal anti-GFP (1:1,000; Aves Labs, Tigard, OR, USA), rabbit polyclonal anti-Prox1 (1:150; GeneTex, Irvine, CA, USA), mouse monoclonal anti-Anxa4 (also named as 2F11; 1:100; Abcam, Cambridge, MA USA), rabbit polyclonal anti-DsRed (1:200; Clontech, Mountain View, CA, USA), rabbit monoclonal anti-DsRed (1:400; Allele Biotechnology, San Diego, CA, USA), goat polyclonal anti-Hnf4a (1:50; Santa Cruz Biotechnology, Dallas, TX, USA), mouse monoclonal anti-Bhmt (1:800; gift from Jinrong Peng at Zhejiang University, P.R. China), mouse monoclonal anti-Alcam (Zn5; 1:10; ZIRC, USA), and conjugated secondary antibodies, including Alexa Fluor 405, 488, 568, and 647 (1:500; Life Technologies, Grand Island, NY, USA).

TUNEL and EdU Assays

Apoptotic cell death was analyzed according to the protocol of the In Situ Cell Death Detection Kit, Fluorescein (Roche, Switzerland). Following whole-mount immunostaining, TUNEL was applied. The 5-ethynyl-2′-deoxyuridine (EdU) assay was performed using the protocol outlined in the Click-iT EdU Alexa Fluor 647 Imaging Kit (Life Technologies). Embryos were treated with egg water containing 10 mM EdU and 10% DMSO from 43 hpf for 1 h and harvested at 45 hpf for EdU staining.

Image Acquisition, Processing, and Statistical Analysis

Zeiss LSM700 confocal and Leica M205 FA epifluorescence microscopes were used to obtain image data. Confocal stacks were analyzed using the Zen 2009 software. All figures, labels, arrows, scale bars, and outlines were assembled or drawn using the Adobe Illustrator software. Unpaired two-tailed Student's *t*-tests in the GraphPad Prism 5 software were used for statistical analysis. A value of $p<0.05$ was considered statistically significant.

RESULTS

tomm22 *Knockdown Initially Reduces Liver Size But Later the Liver Recovers*

The recovery of the initial liver defect in *tomm22* MO-injected larvae, but not in *tomm22* mutants, makes this MO-based assay a novel liver regeneration model[20]. Before we determined the cellular source for this recovery, we carefully examined liver formation in *tomm22* MO-injected embryos and larvae with multiple liver markers. Using the *Tg(fabp10a:GFP)* line that expresses GFP under the hepatocyte-specific *fabp10a* promoter[28], we found that the liver size in the MO-injected larvae was smaller than that in the control larvae at least from 4 dpf (Fig. 1A, arrows). The intensity of *fabp10a:*GFP intrinsic fluorescence was also much weaker in the MO-injected larvae than in the controls until 6 dpf (Fig. 1A). However, at 8 dpf, not only did the *fabp10a:*GFP intensity in the MO-injected larvae recover and appear similar to controls, but the liver size was also greatly increased, compared to the 6-dpf MO-injected liver (Fig. 1A), as previously reported[20]. The MO-injected larvae grew into adults (data not shown), suggesting that the recovered liver is fully functional.

Given the smaller liver of the MO-injected larvae at 4 dpf, we determined whether the liver size was still smaller from the early liver developmental stages. To reveal the entire liver bud during the early stages, we examined the expression of the hepatoblast marker, *prox1a,* and the pan-endoderm marker, *foxa3*[32]. Although, liver bud size was comparable between the control and the MO-injected embryos at 36 hpf, it was noticeably smaller in the MO-injected embryos at 60 hpf (Fig. 1B and C, arrows). In contrast, the pancreas appeared unaffected (Fig. 1C, arrowheads). These data indicate that the initial liver bud formation is grossly normal, but its subsequent growth is defective in *tomm22* MO-injected embryos.

Given the very faint *fabp10a:*GFP expression in *tomm22* MO-injected larvae at 4 and 6 dpf (Fig. 1A), we tested if hepatocyte differentiation was impaired in the MO-injected embryos by examining the expression of the hepatocyte markers *fabp10a, sepp1b*, and *cp*. *fabp10a* expression in the MO-injected embryos at 48 hpf was faint compared to the control embryos (Fig. 1D, arrows), confirming the *fabp10a:*GFP expression pattern. However, *sepp1b* and *cp* expression in the MO-injected embryos was much stronger than *fabp10a* expression in the MO-injected embryos and was comparable with their expression in the controls (Fig. 1D–F, arrows). These data suggest that hepatoblast differentiation into hepatocytes is normal in *tomm22* MO-injected embryos, as observed in *tomm22* mutants[20].

To determine why liver size was reduced upon *tomm22* knockdown, we first examined cell death using terminal deoxynucleotidyl transferase (TdT) dUTP nick-end labeling (TUNEL). TUNEL$^+$ dying cells were not observed in the control liver at 36 hpf or 4 dpf, whereas they were observed in the liver of the MO-injected embryos/larvae at 36 hpf (Fig. 2A) and 4 dpf (Fig. 2B). At 4 dpf, the TUNEL$^+$ cells were hepatocytes, as assessed by hepatocyte *fabp10a:*CFP and BEC *Tp1:*H2B-mCherry expression (Fig. 2B, arrow). We next examined proliferation using EdU labeling. There was no significant difference in the percentage of EdU$^+$ hepatic cells at 45 hpf between the control and the MO-injected embryos (Fig. 2C and D). These data suggest that the small liver in *tomm22* MO-injected embryos is mainly due to increased cell death, consistent with the previous report[20].

BECs Contribute to Hepatocytes in tomm22 *MO-Injected Larvae*

We next determined which cells contributed to the liver recovery in *tomm22* MO-injected larvae. We first examined the hepatic expression of the hepatocyte marker, Hnf4a, and the BEC marker, *Tp1:*H2B-mCherry. The *Tg(Tp1:H2B-mCherry)* line expresses histone H2B (H2B) and mCherry fusion proteins under the promoter containing the notch-responsive element[22]. Since Notch signaling is active in BECs, but not in hepatocytes, *Tp1:*H2B-mCherry expression specifically reveals BECs in the liver[33]. Moreover, H2B makes the H2B-mCherry fusion protein very stable; thus, this line allows for the easy detection of BEC-derived cells even after Notch activity turns off. In fact, in the zebrafish hepatocyte ablation model, BECs exhibit strong H2B-mCherry expression, and BEC-derived hepatocytes exhibit weak H2B-mCherry expression in the regenerating liver[12,25]. In the control larvae, there were no Hnf4a/*Tp1:*H2B-mCherry double-positive cells at 5, 6, and 7 dpf (Fig. 3A and data not shown). In contrast, in the MO-injected larvae at 7 dpf, nearly all Hnf4a$^+$ cells were positive for *Tp1:* H2B-mCherry (Fig. 3A and B), suggesting their biliary origin. To determine when these double-positive cells first appeared, we examined earlier stages and found that such double-positive cells appeared in a subset of the MO-injected larvae at 5 dpf (Fig. 3A, arrows). The formation of the double-positive cells can be explained in two ways: (1) *Tp1:*H2B-mCherry$^+$ BECs turn on Hnf4a expression, suggesting BEC conversion to hepatocytes,

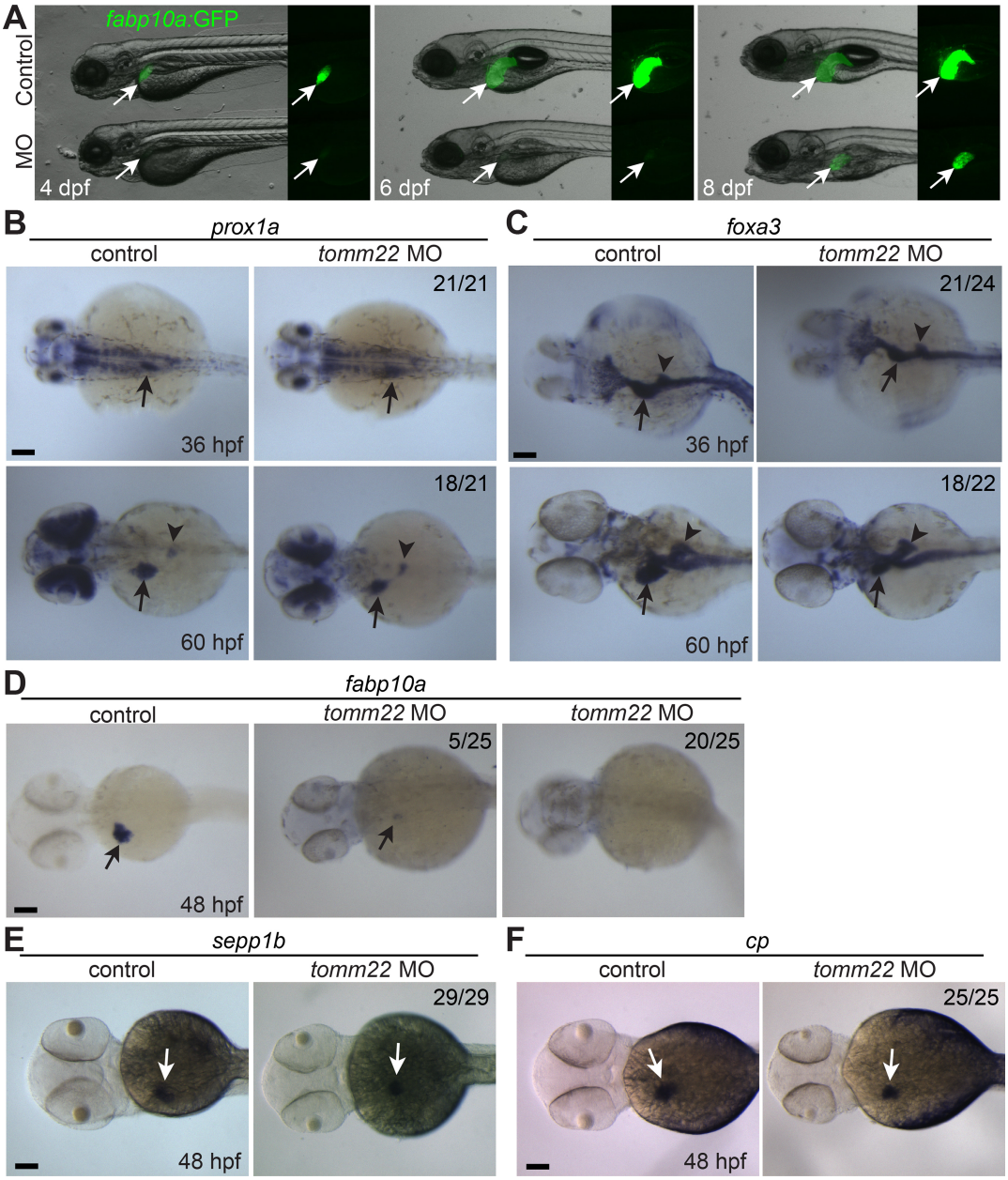

Figure 1. *tomm22* knockdown reduces liver size. (A) Fluorescence images showing hepatic *fabp10a:*GFP expression (arrows) in *tomm22* MO-injected larvae. Note very weak *fabp10a:*GFP expression until 6 days postfertilization (dpf) but its strong expression at 8 dpf. (B–E) Whole-mount in situ hybridization images showing the expression of *prox1a, foxa3*, *fabp10a, sepp1b*, and *cp* in the MO-injected embryos. Numbers indicate the proportion of larvae exhibiting the representative expression shown. Arrows point to the liver bud or the liver; arrowheads point to the dorsal pancreas. Scale bars: 100 μm.

or (2) Hnf4a^{+} hepatocytes turn on *Tp1:*H2B-mCherry expression, suggesting the formation of hybrid hepatocytes. To unambiguously determine the origin of hepatocytes in the recovering liver of the MO-injected larvae, we performed permanent lineage tracing experiments using the Cre/loxP system. To trace BEC lineage, we used the *Tg(Tp1:CreERT2)* line together with a Cre reporter line, *Tg(ubb:loxP-GFP-STOP-loxP-mCherry)*, which expresses mCherry upon Cre-mediated excision of the *STOP* cassette[23]. 4-OHT was treated from 48 to 84 hpf, the stage before the appearance of *Tp1:*H2B-mCherry/Hnf4a double-positive cells. In the control larvae, only BECs were labeled with mCherry, as previously reported[12]. In sharp contrast, in the MO-injected larvae, numerous hepatocytes were labeled with mCherry at 9 dpf (Fig. 3C), indicating their biliary origin. However,

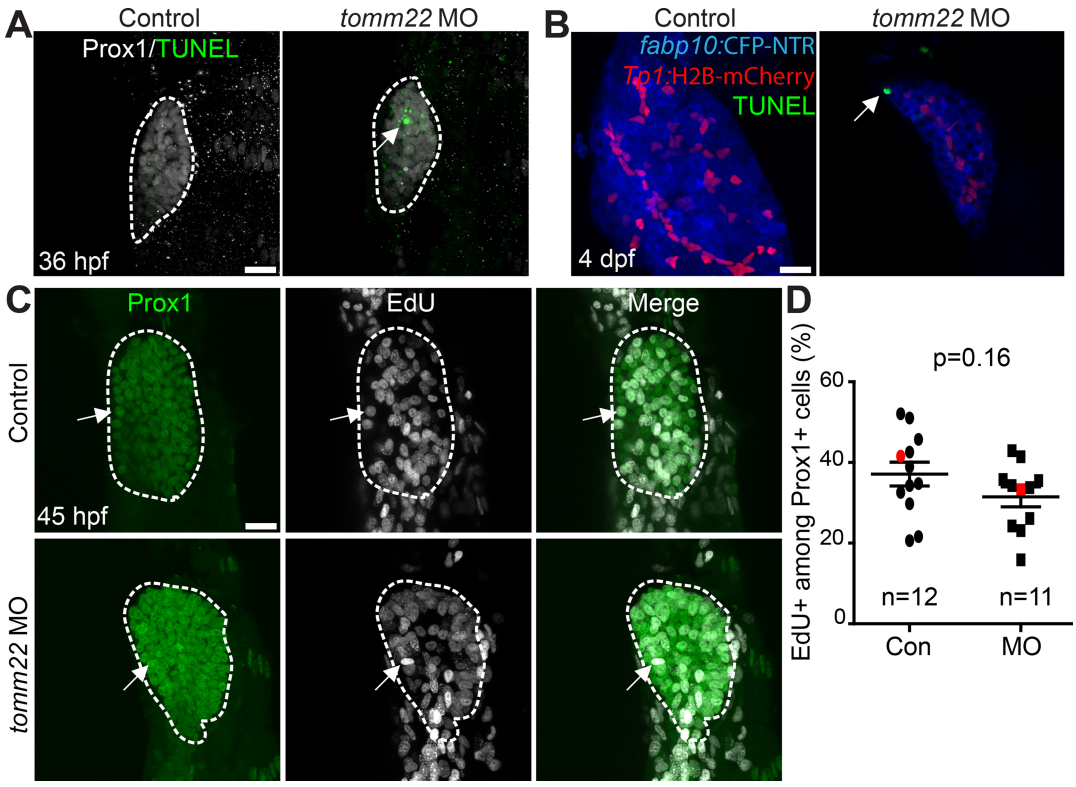

Figure 2. Cell death and proliferation in *tomm22* MO-injected larvae. (A) Confocal projection images showing Prox1 expression (gray) and terminal deoxynucleotidyl transferase (TdT) dUTP nick-end labeling (TUNEL) (green) in the liver bud (dashed lines) at 36 h postfertilization (hpf). Arrow points to TUNEL$^+$ cells. (B) Confocal projection images showing TUNEL (green) and the expression of *fabp10a:*CFP-NTR (blue) and *Tp1:*H2B-mCherry (red) in the liver at 4 dpf. Arrow points to TUNEL$^+$ hepatocytes. (C) Confocal projection images showing Prox1 expression (green) and 5-ethynyl-2′-deoxyuridine (EdU) labeling (gray) in the liver (dashed lines) at 45 hpf. Arrows point to EdU/Prox1 double-positive cells. (D) Graph showing the percentage of EdU$^+$ cells among Prox1$^+$ cells in the liver at 45 hpf. There was no significant difference in the proliferation rate between the control and *tomm22* MO-injected larvae. Red marks indicate the embryos shown in (C); *n* indicates the number of larvae examined. Scale bars: 20 μm; error bars: ±SEM.

about 40% of hepatocytes were labeled with mCherry with the range of 0–60% (Fig. 3D). Although 66% of the Cre-mediated labeling efficiency in the MO-injected larvae at 9 dpf (Fig. 3E) can explain, in part, such a low percentage, the percentage is still low compared with the percentage of *Tp1:*H2B-mCherry$^+$ cells among Hnf4a$^+$ cells (~100%) at 7 dpf (Fig. 3D vs. Fig. 3B), suggesting the contribution of non-BECs to recovering hepatocytes in *tomm22* MO-injected larvae. These lineage tracing data reveal that both BECs and non-BECs, most likely surviving hepatocytes, give rise to recovered hepatocytes in *tomm22* MO-injected larvae.

Surviving Hepatocytes Become Hybrid Hepatocytes in tomm22 *MO-Injected Larvae*

Our lineage tracing data suggest that surviving hepatocytes turned on *Tp1:*H2B-mCherry expression in *tomm22* MO-injected larvae. Since Notch signaling is required and sufficient for biliary specification[34,35] and is required for the conversion of hepatocytes to BECs[7], the hepatocyte induction of *Tp1:*H2B-mCherry can be considered the formation of hybrid hepatocytes expressing biliary markers. We investigated if such hybrid cells indeed formed in *tomm22* MO-injected larvae. We assumed that if hepatocytes start to express *Tp1:*H2B-mCherry, its expression should be very faint at the beginning. By focusing on such faint expression with the increase in gain in confocal microscopy, we could detect a few hepatocytes exhibiting the extremely faint expression of *Tp1:*H2B-mCherry in the MO-injected larvae at 4 dpf (Fig. 4A, arrows). The expression of the hepatocyte differentiation marker, Bhmt[36], was used to distinguish hepatocytes from BECs. At 4 dpf, *Tp1:*H2B-mCherry expression in Bhmt$^+$ hepatocytes was much weaker than its expression in Bhmt$^-$ BECs, whereas, at 6 dpf, its expression level was comparable with that in Bhmt$^-$ BECs (Fig. 4A, arrows vs. arrowheads). Since BEC markers are expressed in hybrid hepatocytes in mice[4,5,7], we next examined the expression of another BEC marker, Anxa4[33], and found that Anxa4 was also expressed in most *Tp1:*H2B-mCherry$^+$ cells in the MO-injected larvae at 6 dpf (Fig. 4B, arrows).

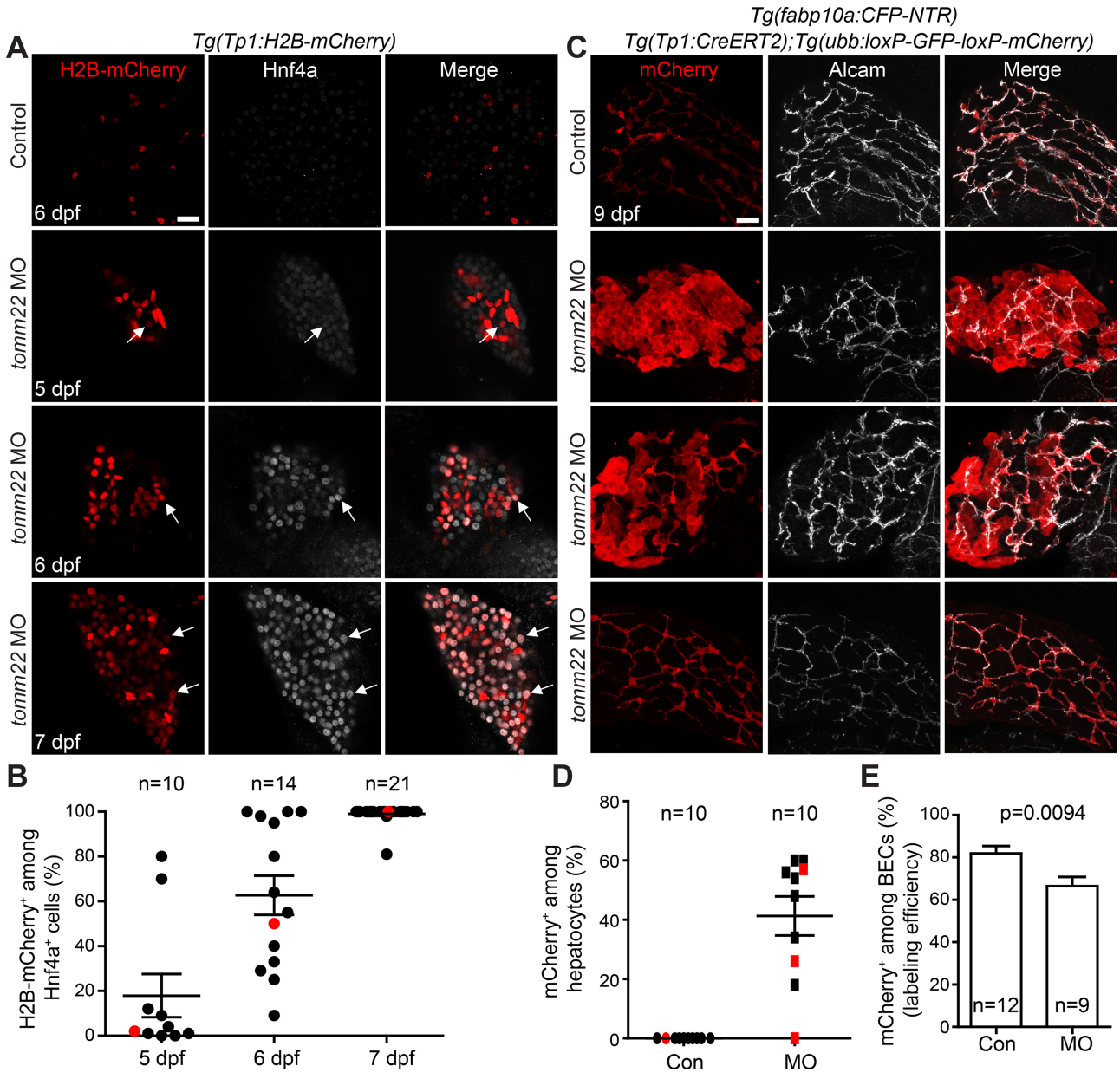

Figure 3. Biliary epithelial cells (BECs) give rise to hepatocytes in *tomm22* MO-injected larvae. (A) Confocal single-optical section images showing *Tp1:*H2B-mCherry (red) and Hnf4a (gray) expression in the liver. Arrows point to H2B-mCherry/Hnf4a double-positive cells. (B) A graph showing the percentage of H2B-mCherry$^+$ cells among Hnf4a$^+$ cells in the livers of the *tomm22* MO-injected larvae. Red dots indicate the larvae shown in (A). (C) Confocal projection images showing the hepatic expression of *ubb:*mCherry (red, Cre-labeled cells) and Alcam (gray, BECs) at 9 dpf. 4-OHT was treated from 48 to 84 hpf. (D) Graph showing the percentage of *ubb:*mCherry$^+$ hepatocytes, which were derived from BECs. *fabp10a:*CFP-NTR expression was used to define hepatocytes. Red marks indicate the larvae shown in (C). (E) Graph showing the percentage of mCherry$^+$ cells among Alcam$^+$ BECs at 9 dpf, indicating Cre-mediated labeling efficiency. *n* indicates the number of larvae examined. Scale bars: 20 μm; error bars: ±SEM.

If BECs or BEC-derived cells do not express Hnf4a at 4–5 dpf, it will indirectly indicate that the H2B-mCherry/Hnf4a double-positive cells at these stages are derived from hepatocytes. Thus, we performed BEC lineage tracing experiments and examined Hnf4a expression in lineage-traced, MO-injected larvae at 4–8 dpf. The Cre-labeled, mCherry$^+$ cells did not express Hnf4a until 5 dpf, but from 6 dpf, a subset of these cells expressed Hnf4a (Fig. 4C and D). These data together with the *Tp1:*H2B-mCherry expression data indicate that surviving hepatocytes become hybrid hepatocytes and contribute to recovering hepatocytes in *tomm22* MO-injected larvae.

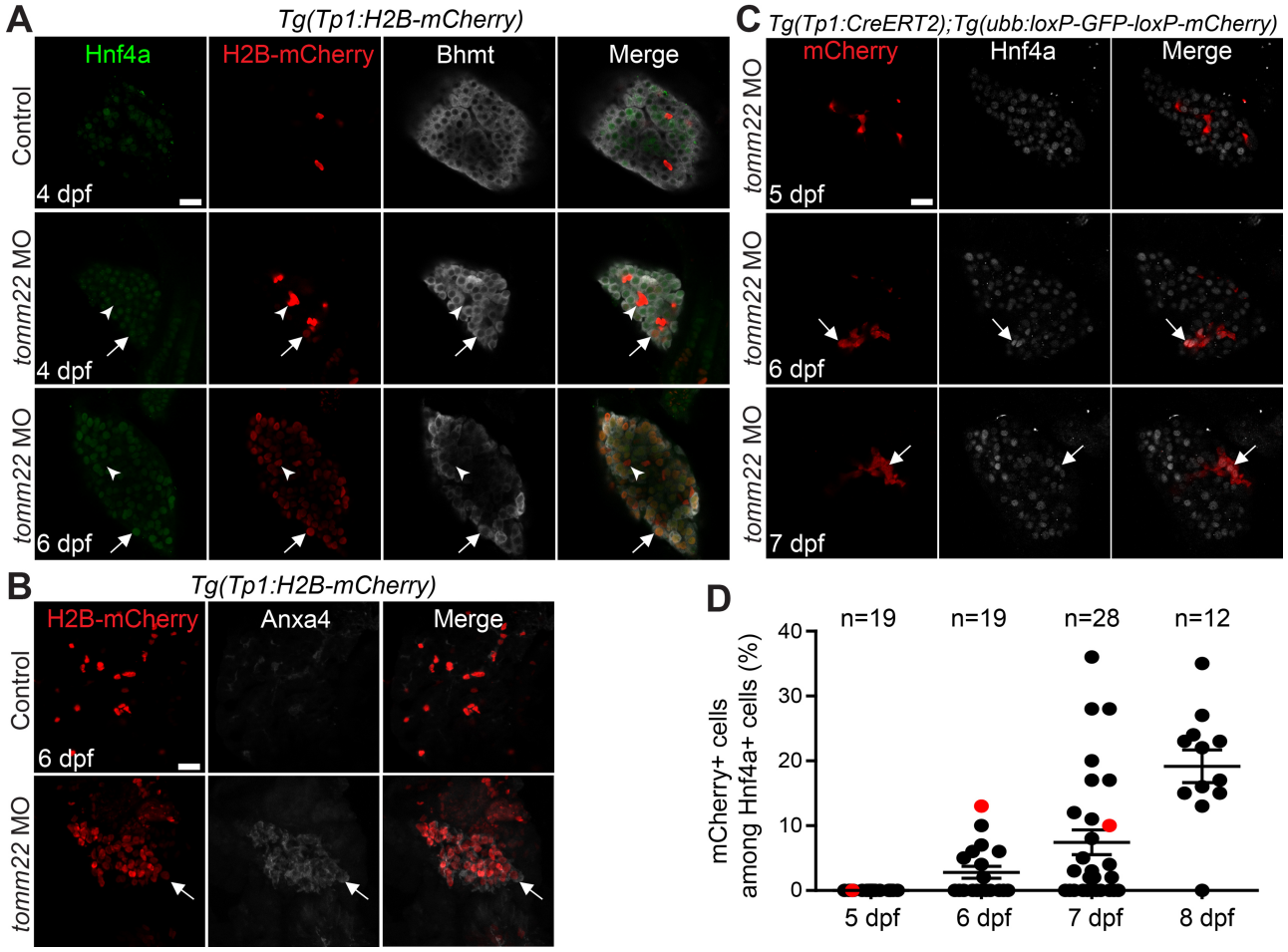

Figure 4. Surviving hepatocytes become hybrid hepatocytes. (A) Confocal single-optical section images showing the expression of Hnf4a (green), *Tp1:*H2B-mCherry (red), and Bhmt (gray) in the liver. Arrows point to hepatocytes that express *Tp1:*H2B-mCherry; arrowheads point to BECs negative for Hnf4a and Bhmt. (B) Confocal projection images showing *Tp1*:H2B-mCherry (red) and Anxa4 (gray) expression in the liver. Arrows point to H2B-mCherry/Anxa4 double-positive cells. (C) Confocal single-optical section images showing the hepatic expression of *ubb*:mCherry (red, Cre-labeled cells) and Hnf4a (gray) in *tomm22* MO-injected larvae. Arrows point to mCherry/Hnf4a double-positive cells. (D) Graph showing the percentage of *ubb:*mCherry^{+} cells among Hnf4a^{+} cells, which were derived from BECs. Red dots indicate the larvae shown in (C); *n* indicates the number of larvae examined. Scale bars: 20 μm; error bars: ±SEM.

Suppression of Wnt/β-Catenin Signaling Blocks Hepatocyte Proliferation and Represses the Formation of Hybrid Hepatocytes in tomm22 *MO-Injected Larvae*

It was previously reported that Wnt/β-catenin signaling positively regulates liver recovery in *tomm22* MO-injected larvae[20]. A Wnt ligand gene, *wnt2bb*, was upregulated in the livers of the MO-injected larvae, and the suppression of Wnt/β-catenin signaling reduced the size of the recovering livers of the MO-injected larvae[20]. Since Wnt/β-catenin signaling regulates hepatocyte proliferation during liver regeneration[37], we sought to determine if the reduced liver recovery upon Wnt suppression was due to a proliferation defect. We first examined if Wnt activity was enhanced in *tomm22* MO-injected larvae. Using a Wnt reporter line, *Tg(WRE:d2GFP)*[26], we observed a strong *WRE:*d2GFP expression in the livers of *tomm22* MO-injected larvae at 6 dpf, but no expression in the control livers (Fig. 5A). About 60% of *Tp1:*H2B-mCherry^{+} cells exhibited Wnt activity in the livers of the MO-injected larvae. We next suppressed Wnt/β-catenin signaling by treating *tomm22* MO-injected larvae from 4 to 7 dpf with a Wnt inhibitor, XAV939, which stimulates β-catenin degradation by stabilizing Axin[38] (Fig. 5B). As reported previously[20], the suppression of Wnt/β-catenin signaling reduced the size of the recovering liver in the MO-injected larvae. Consistent with the positive role of Wnt/β-catenin signaling in hepatocyte proliferation during liver regeneration[37], XAV939 treatment greatly reduced hepatocyte proliferation in *tomm22* MO-injected larvae at 7 dpf compared with the DMSO treatment control

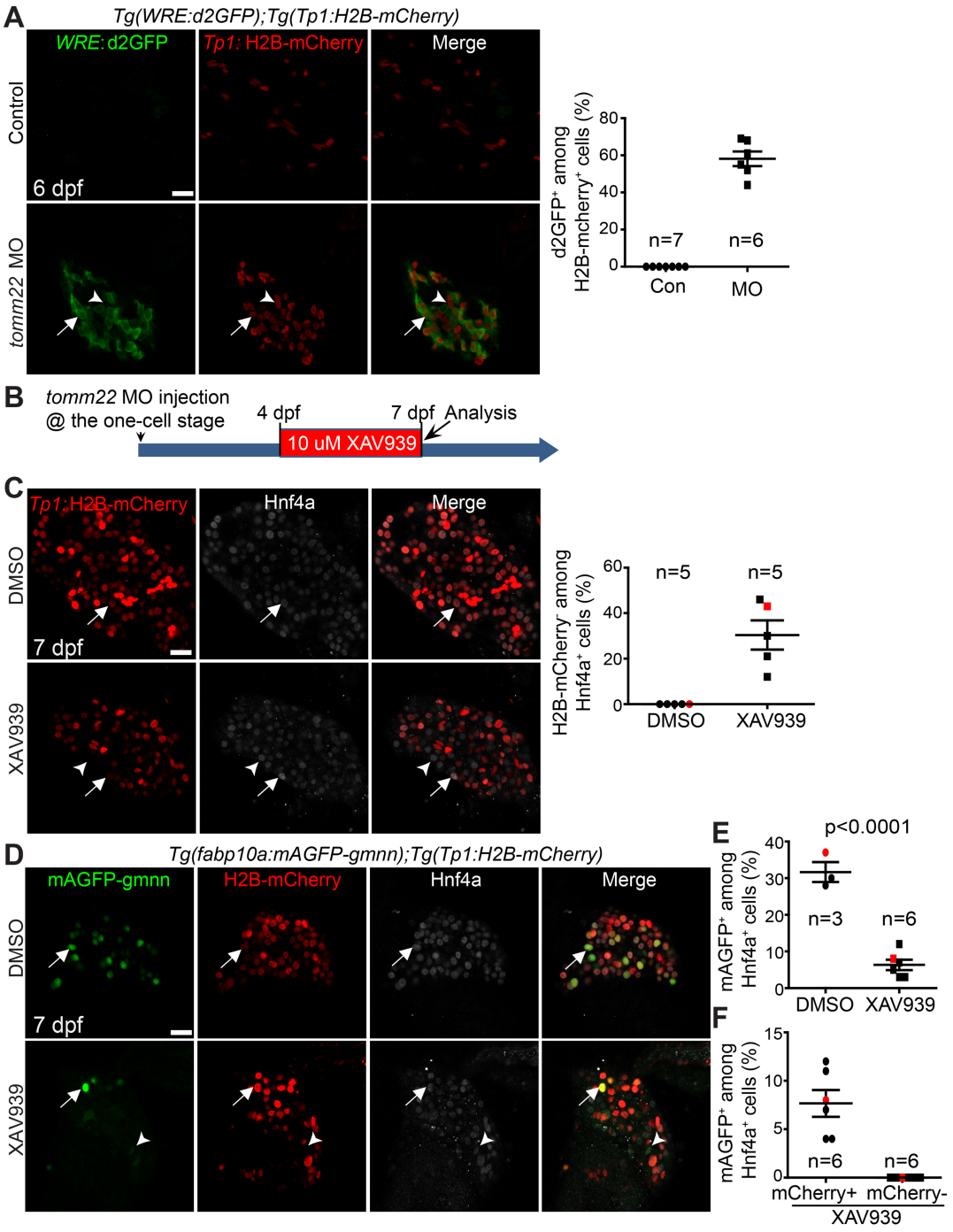

Figure 5. Suppression of Wnt/β-catenin signaling represses hepatocyte proliferation and the formation of hybrid hepatocytes in *tomm22* MO-injected larvae. (A) Confocal single-optical section images showing *WRE*:d2GFP (green) and *Tp1*:H2B-mCherry (red) expression in the liver at 6 dpf. Arrows point to d2GFP/H2B-mCherry double-positive cells; arrowheads point to H2B-mCherry single-positive cells. Quantification of the percentage of d2GFP$^+$ cells among H2B-mCherry$^+$ cells is shown. (B) Scheme illustrating the period of XAV939 treatment for (C)–(F). (C) Confocal single-optical section images showing the hepatic expression of *Tp1*:H2B-mCherry (red) and Hnf4a (gray) at 7 dpf. Arrows point to H2B-mCherry/Hnf4a double-positive cells; arrowheads point to H2B-mCherry$^-$/Hnf4a$^+$ cells. Quantification of the percentage of H2B-mCherry$^-$ cells among Hnf4a$^+$ cells is shown. (D) Confocal single-optical images showing the hepatic expression of *fabp10a*:mAGFP-gmnn (green), *Tp1*:H2B-mCherry (red), and Hnf4a (gray) at 7 dpf. Arrows point to mAGFP-gmnn/H2B-mCherry/Hnf4a triple-positive cells; arrowheads point to mAGFP-gmnn/Hnf4a double-positive cells. (E) Graph showing the percentage of mAGFP-gmnn$^+$ cells among Hnf4a$^+$ cells. Red marks indicate the larvae shown in (D). (F) Graph showing the percentage of mCherry$^+$ or mCherry$^-$ proliferating hepatocytes. Red marks indicate the larvae shown in (D). *n* indicates the number of larvae examined. Scale bars: 20 μm; error bars: ±SEM.

(Fig. 5D and E). For the proliferation assay, we used the *Tg(fabp10a:mAGFP-gmnn)* line[25], which expresses green fluorescent proteins in hepatocytes that are in the S/G_2/M, but not in the G_0 or G_1, phases of the cell cycle[39]. In addition to this proliferation phenotype, we intriguingly observed a novel phenotype, the presence of Hnf4a$^+$ cells negative for *Tp1:*H2B-mCherry (Fig. 5C and D, arrowheads). About 30% of Hnf4a$^+$ cells were negative for *Tp1:*H2B-mCherry in XAV939-treated, *tomm22* MO-injected larvae at 7 dpf, whereas none of such cells were present in the DMSO-treated, MO-injected larvae (Fig. 5C). Since BEC-derived hepatocytes retain *Tp1:*H2B-mCherry expression, it is likely that a subset of surviving, preexisting hepatocytes failed to turn on *Tp1:*H2B-mCherry expression in the XAV939-treated, MO-injected larvae. Interestingly, the proliferation assay with the *Tg(fabp10a:mAGFP-gmnn)* line revealed that *Tp1:*H2B-mCherry$^-$/Hnf4a$^+$ hepatocytes were more sensitive to Wnt/β-catenin inhibition than *Tp1:*H2B-mCherry$^+$/Hnf4a$^+$ hepatocytes because the proliferation rate of the former cells was much lower than that of the latter (0% vs. 6%) (Fig. 5F). Altogether, these data suggest that in *tomm22* MO-injected larvae, Wnt/β-catenin signaling promotes the formation of hybrid hepatocytes as well as hepatocyte proliferation.

Macrophage Ablation Impairs the Formation of Hybrid Hepatocytes in tomm22 *MO-Injected Larvae*

Given the positive role of macrophages in oval cell activation[40] and oval cell differentiation into hepatocytes[41] in mice, we sought to determine the role of macrophages in *tomm22* MO-mediated liver regeneration. We first examined if macrophages were present in the livers of *tomm22* MO-injected larvae. Using the *Tg(mpeg1:Dendra2)* line that expresses a fluorescent protein Dendra2 under the macrophage-specific *mpeg1* promoter[29], we first detected macrophages in the livers of *tomm22* MO-injected larvae at 5 dpf (Fig. 6A, arrows) and observed more macrophages at 7 dpf (Fig. 6B). We often observed macrophages surrounding *Tp1:*H2B-mCherry$^-$ hepatocytes (Fig. 6B, arrowheads) but barely detected macrophages surrounding *Tp1:*H2B-mCherry$^+$ hepatocytes. In the control liver, a few macrophages were also detected at 7 dpf, but their shape was different from that of the MO-injected larvae: macrophages in the control liver were elongated, whereas those in the MO-injected larvae were spherical (Fig. 6A and B). Given the increased number of macrophages in the livers of *tomm22* MO-injected larvae and their shape change, we next investigated the effect of macrophage ablation on *tomm22* MO-mediated liver regeneration. Using two transgenic lines that make NTR specifically expressed in macrophages[42], *Tg(mpeg1:Gal4-VP16)* and *Tg(UAS:NTR-mCherry)*, we ablated macrophages by treating the double transgenic larvae with Mtz. Since macrophages were detected in the livers of the MO-injected larvae from 5 dpf (Fig. 6A), we applied Mtz from 4 to 7 dpf and examined the liver at 7 dpf (Fig. 6D). This Mtz treatment greatly reduced the number of macrophages in the whole body of the transgenic larvae at 7 dpf, as assessed by NTR-mCherry intrinsic fluorescence (Fig. 6C), validating efficient macrophage ablation with the NTR/Mtz system. Intriguingly, we observed the presence of *Tp1:*H2B-mCherry$^-$/Hnf4a$^+$ hepatocytes following macrophage ablation in *tomm22* MO-injected larvae (Fig. 6E, arrowheads), similar to our observations in XAV939-treated, MO-injected larvae (Fig. 5C). All Hnf4a$^+$ cells were positive for *Tp1:*H2B-mCherry in the DMSO-treated, MO-injected larvae, whereas 67% of them were negative for *Tp1:*H2B-mCherry (Fig. 6F), suggesting a defect in the formation of hybrid hepatocytes. However, unlike XAV939 treatment, macrophage ablation did not reduce the proliferation of Hnf4a$^+$ hepatocytes (Fig. 6G and H). Moreover, *Tp1:*H2B-mCherry$^-$/Hnf4a$^+$ hepatocytes proliferated more than *Tp1:*H2B-mCherry$^+$/Hnf4a$^+$ hepatocytes (Fig. 6I). Given the possibility that macrophages regulate Wnt/β-catenin signaling[41], using the *Tg(WRE:d2GFP*) line, we examined Wnt activity in macrophage-ablated, *tomm22* MO-injected larvae. Hepatic *WRE:*d2GFP expression was greatly reduced in the macrophage-ablated, MO-injected larvae compared with unablated, MO-injected larvae (Fig. 6J), supporting the possibility that macrophages regulate Wnt/β-catenin signaling during *tomm22* MO-mediated liver regeneration. Altogether, these data suggest that during *tomm22* MO-mediated liver regeneration, macrophages do not control hepatocyte proliferation but regulate the formation of hybrid hepatocytes, in part, via Wnt/β-catenin signaling.

DISCUSSION

In this study, we determined the origin of hepatic cells that contribute to recovering hepatocytes in *tomm22* MO-injected larvae. By temporarily knocking down *tomm22*, we observed the initial reduction of liver size as a result of hepatocyte cell death. This liver damage not only activated BECs to give rise to hepatocytes but also induced the phenotypic change of surviving hepatocytes, generating hybrid hepatocytes. Upon MO dilution as larvae grow, hepatocytes arising from either surviving hepatocytes or BECs began to form properly, allowing for the survival of the MO-injected larvae. Using this MO-based liver regeneration model, we discovered that both Wnt/β-catenin signaling and macrophages control the formation of hybrid hepatocytes.

In *tomm22* MO-injected larvae at 7 dpf, nearly all Hnf4a$^+$ cells expressed *Tp1:*H2B-mCherry (Fig. 3B). However, permanent BEC lineage tracing data show that about 7% of Hnf4a$^+$ cells, with the range of 0–36%, were derived from BECs at 7 dpf (Fig. 4D). Even considering ~66% Cre

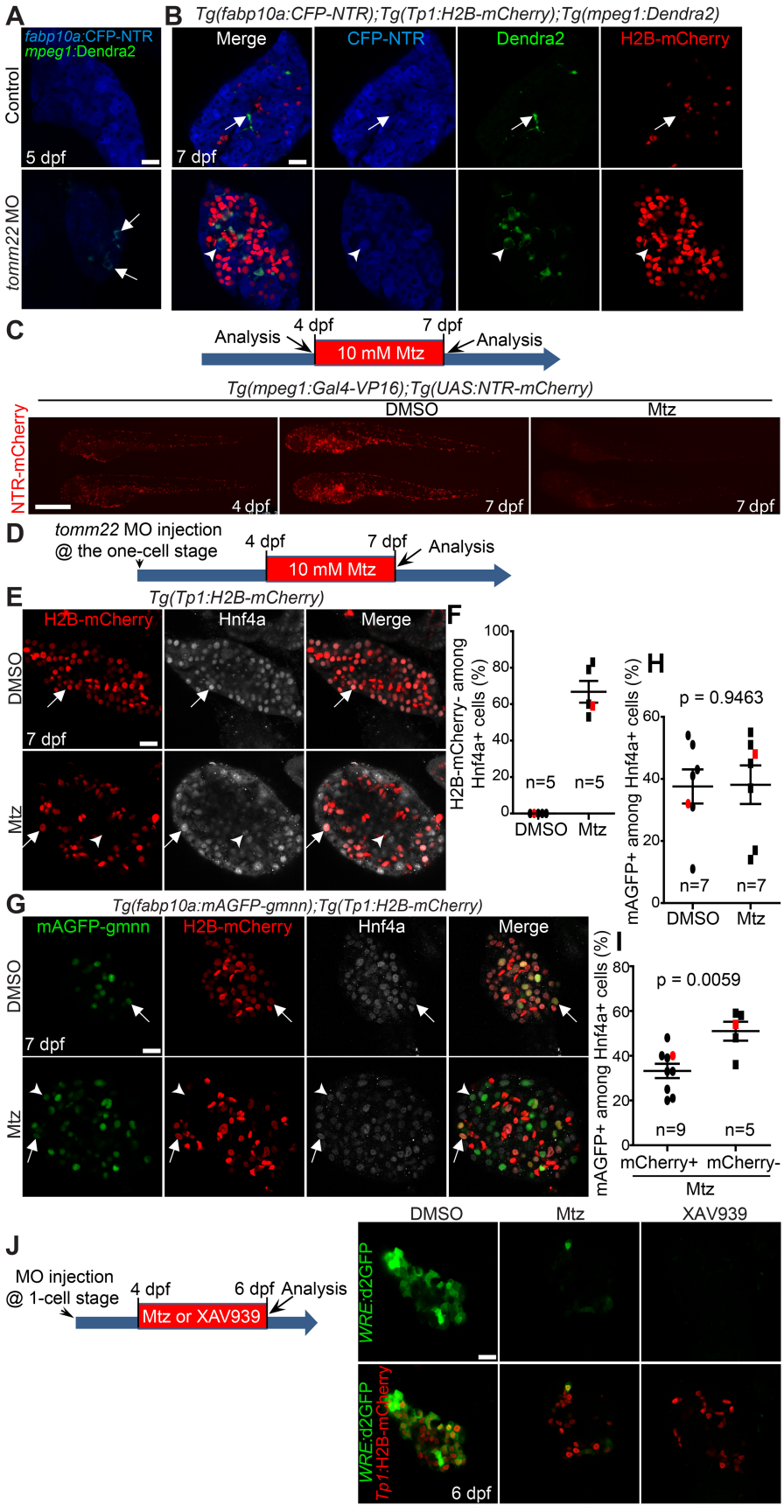
A
fabp10a:CFP-NTR
mpeg1:Dendra2
Control
tomm22 MO
5 dpf
B
Tg(fabp10a:CFP-NTR);Tg(Tp1:H2B-mCherry);Tg(mpeg1:Dendra2)
Merge
CFP-NTR
Dendra2
H2B-mCherry
7 dpf
C
Analysis
4 dpf
7 dpf
10 mM Mtz
Analysis
Tg(mpeg1:Gal4-VP16);Tg(UAS:NTR-mCherry)
DMSO
Mtz
NTR-mCherry
4 dpf
7 dpf
7 dpf
D
tomm22 MO injection
@ the one-cell stage
4 dpf
7 dpf
Analysis
10 mM Mtz
E
Tg(Tp1:H2B-mCherry)
H2B-mCherry
Hnf4a
Merge
DMSO
Mtz
7 dpf
F
H2B-mCherry- among Hnf4a+ cells (%)
n=5
n=5
DMSO
Mtz
H
p = 0.9463
mAGFP+ among Hnf4a+ cells (%)
n=7
n=7
DMSO
Mtz
G
Tg(fabp10a:mAGFP-gmnn);Tg(Tp1:H2B-mCherry)
mAGFP-gmnn
H2B-mCherry
Hnf4a
Merge
DMSO
Mtz
7 dpf
I
p = 0.0059
mAGFP+ among Hnf4a+ cells (%)
n=9
n=5
mCherry+
mCherry-
Mtz
J
MO injection
@ 1-cell stage
4 dpf
6 dpf
Analysis
Mtz or XAV939
DMSO
Mtz
XAV939
WRE:d2GFP
WRE:d2GFP
Tp1:H2B-mCherry
6 dpf

labeling efficiency in the MO-injected larvae (Fig. 3E), these data suggest that a large subset of Hnf4a/*Tp1:*H2B-mCherry double-positive cells were derived from non-BECs. Our finding that most of the double-positive cells expressed the hepatocyte differentiation marker, Bhmt (Fig. 4A), and the BEC marker, Anxa4 (Fig. 4B), in the livers of *tomm22* MO-injected larvae at 6 dpf supports that hepatocytes become hybrid hepatocytes in the MO-injected larvae. These hybrid hepatocytes were frequently observed in diverse murine liver injury models. In particular, hepatocyte lineage tracing studies in mice revealed that upon chronic liver injuries, a subset of hepatocytes convert to oval cells, which express both hepatocyte and biliary markers and later redifferentiate into hepatocytes[4,6–8]. This hepatocyte conversion and redifferentiation appear to occur in *tomm22* MO-injected larvae as well.

We previously reported that injury levels determine the mode of liver regeneration between hepatocyte- and BEC-driven liver regeneration[12]. Upon mild hepatocyte ablation, only preexisting hepatocytes contribute to regenerating hepatocytes, whereas upon near-total hepatocyte ablation, BECs contribute to hepatocytes without the contribution of preexisting hepatocytes. Intriguingly, upon intermediate hepatocyte ablation, both hepatocytes and BECs appear to contribute to regenerating hepatocytes[12]. This relationship between liver injury levels and the mode of liver regeneration observed in zebrafish is supported by mouse studies. In mouse oval cell activation models, including CCl_4 injection and DDC and CDE diet, preexisting hepatocytes, but not BECs, contribute to regenerating hepatocytes[4–8]. Since remaining hepatocytes actively proliferate in these liver injury models, liver injury levels can be considered "mild" in these models. However, when liver injury is very severe, that is, remaining hepatocytes cannot proliferate, BECs extensively contribute to regenerating hepatocytes. This phenomenon was recently observed in hepatocyte-specific *Mdm2* knockout mice[9]. Given the dual contribution of surviving, preexisting hepatocytes and BECs to recovering hepatocytes in *tomm22* MO-injected larvae, liver injury levels in this MO-based liver injury model can be considered "intermediate." In fact, 2 ng of *tomm22* MO injection appeared to elicit a mild liver injury because the liver size in the MO-injected larvae was smaller than in the controls but larger than in larvae injected with 6 ng of the MO. Importantly, in the larvae injected with 2 ng of the MO, we did not observe any BEC contribution to hepatocytes (data not shown), further supporting the relationship between liver injury levels and the mode of liver regeneration.

Wnt/β-catenin signaling promotes hepatocyte proliferation during liver regeneration[37], and in chronic liver injury settings, such as the CDE diet, Wnt/β-catenin signaling also appears to promote the differentiation of liver progenitor cells into hepatocytes[41]. Here we confirmed the positive effect of Wnt/β-catenin signaling on hepatocyte proliferation in *tomm22* MO-injected larvae by (1) showing the enhanced Wnt activity in the MO-injected livers and (2) reporting that hepatocyte proliferation was greatly reduced in XAV939-treated, MO-injected larvae compared with DMSO-treated, MO-injected larvae. Moreover, we found a novel phenotype in XAV939-treated, recovering livers: the presence of Hnf4a$^+$ cells negative for *Tp1:*H2B-mCherry. Since BEC-derived Hnf4a$^+$ cells retain *Tp1:*H2B-mCherry expression due to the long half-life of H2B-mCherry proteins, the Hnf4a single-positive cells should be derived from surviving hepatocytes. Given that nearly all Hnf4a$^+$ cells were positive for *Tp1:*H2B-mCherry in *tomm22* MO-injected larvae at 7 dpf (Fig. 3B), the presence of the single-positive cells suggests that the suppression of Wnt/β-catenin signaling

FACING PAGE

Figure 6. Macrophage ablation impairs the formation of hybrid hepatocytes in *tomm22* MO-injected larvae. (A) Confocal single-optical section images showing the expression of *mpeg1:*Dendra2 (green, macrophages) and *fabp10a:*CFP-NTR (blue, hepatocytes) in the liver at 5 dpf. Arrows point to macrophages. (B) Confocal single-optical section images showing the expression of *mpeg1:*Dendra2 (green), *Tp1:*H2B-mCherry (red), and *fabp10a:*CFP-NTR (blue) in the liver at 7 dpf. Arrows point to macrophages in the control liver; arrowheads point to a macrophage engulfing a hepatocyte in *tomm22* MO-injected larvae. (C) Fluorescence images showing macrophage NTR-mCherry expression before and after metronidazole (Mtz) treatment. Mtz (10 mM) was treated from 4 to 7 dpf. Note the great reduction in the number of NTR-mCherry$^+$ macrophages in the Mtz-treated larvae at 7 dpf compared with the DMSO-treated controls. Lateral views, dorsal up, anterior to the left. Scale bar: 250 μm. (D) Scheme illustrating the period of Mtz treatment and harvest stage for macrophage ablation for (E–I). (E) Confocal single-optical section images showing the expression of *Tp1*:H2B-mCherry (red) and Hnf4a (gray) in the liver at 7 dpf. Arrows point to H2B-mCherry/Hnf4a double-positive cells; arrowheads point to Hnf4a single-positive cells. (F) Graph showing the percentage of H2B-mCherry$^-$ cells among Hnf4a$^+$ cells. Red marks indicate the larvae shown in (E). (G) Confocal single-optical section images showing the expression of *fabp10a*:mAGFP-gmnn (green), *Tp1*:H2B-mCherry (red), and Hnf4a (gray) in the liver at 7 dpf. Arrows point to mAGFP-gmnn/H2B-mCherry/Hnf4a triple-positive cells; arrowheads point to mAGFP-gmnn$^+$/H2B-mCherry$^-$/Hnf4a$^+$ cells. (H) Graph showing the percentage of *fabp10a:*mAGFP-gmnn$^+$ cells among Hnf4a$^+$ cells. Red marks indicate the larvae shown in (G). (I) Graph showing the percentage of H2B-mCherry$^+$ or H2B-mCherry$^-$ proliferating Hnf4a$^+$ cells. Red marks indicate the larvae shown in (G). *n* indicates the number of larvae examined. (J) Confocal single-optical section images showing the expression of *WRE*:d2GFP (green, Wnt activity) and *Tp1:*H2B-mCherry (red) in the liver at 6 dpf. Anti-GFP antibody was used to reveal *WRE:*d2GFP expression. Note the complete absence of hepatic d2GFP expression in the XAV939-treated, *tomm22* MO-injected larvae, whereas its faint expression in macrophage-ablated, *tomm22* MO-injected larvae. Scale bars: 20 μm, except (C); error bars: ±SEM.

represses *Tp1:H2B-mCherry* induction in hepatocytes (i.e., the formation of hybrid hepatocytes). This suggestion is supported by a recent mouse study showing that Wnt/β-catenin signaling induces the expression of biliary markers, such as Sox9, EpCAM, and CK19, in hepatocytes[43]. Intriguingly, we found a similar phenotype in the MO-injected larvae upon macrophage ablation. Our finding that hepatic Wnt activity was greatly reduced in *tomm22* MO-injected larvae with macrophage ablated compared with the unablated MO-injected larvae (Fig. 6J) suggests that macrophages may promote the formation of hybrid hepatocytes, in part, via Wnt/β-catenin signaling. This hypothesis is consistent with a mouse study showing that in the CDE model, macrophage engulfment of dying hepatocytes and their debris induces Wnt3a expression[41]. However, the number of $Hnf4a^+$ cells negative for *Tp1:*H2B-mCherry was doubled upon macrophage ablation compared with XAV939 treatment (67% vs. 30%), suggesting the involvement of other factors from macrophages in the formation of hybrid hepatocytes.

Despite the reduced Wnt activity in the recovering livers of the macrophage-ablated, MO-injected larvae, hepatocyte proliferation was not affected at all, making a sharp contrast with the great reduction of hepatocyte proliferation in the XAV939-treated, MO-injected larvae (Fig. 5E vs. Fig. 6H). The direct comparison of hepatic Wnt activity between these two cases revealed no Wnt activity in the XAV939-treated, MO-injected larvae but faint Wnt activity in the macrophage-ablated, MO-injected larvae (Fig. 6J). These data suggest that the remaining Wnt activity in the macrophage-ablated larvae may be sufficient for hepatocyte proliferation.

In summary, here we report an additional zebrafish liver injury model for BEC-driven liver regeneration. Together with the NTR/Mtz-mediated hepatocyte ablation model, this *tomm22* MO-based liver injury model will help elucidate the mechanisms underlying BEC-driven liver regeneration, providing insights into augmenting innate liver regeneration in patients with advanced liver diseases.

ACKNOWLEDGMENTS: The authors thank Jinrong Peng for anti-Bhmt antibody, Neil Hukriede and Michael Tsang for discussion, and Mehwish Khaliq for the critical reading of the manuscript. The authors also thank Juhoon So for his confirmative experiments with tomm22 *MO. The work was supported by a grant from the NIH to D.S. (R01DK101426). J.W. is a visiting research scholar at the University of Pittsburgh and was supported from the China Scholarship Council. The authors declare no conflicts of interest.*

REFERENCES

1. Michalopoulos GK. Liver regeneration after partial hepatectomy: Critical analysis of mechanistic dilemmas. Am J Pathol. 2010;176(1):2–13.
2. Duncan AW, Dorrell C, Grompe M. Stem cells and liver regeneration. Gastroenterology 2009;137(2):466–81.
3. Fausto N, Campbell JS. The role of hepatocytes and oval cells in liver regeneration and repopulation. Mech Dev. 2003;120(1):117–30.
4. Yanger K, Knigin D, Zong YW, Maggs L, Gu GQ, Akiyama H, Pikarsky E, Stanger BZ. Adult hepatocytes are generated by self-duplication rather than stem cell differentiation. Cell Stem Cell 2014;15(3):340–9.
5. Tarlow BD, Pelz C, Naugler WE, Wakefield L, Wilson EM, Finegold MJ, Grompe M. Bipotential adult liver progenitors are derived from chronically injured mature hepatocytes. Cell Stem Cell 2014;15(5):605–18.
6. Schaub JR, Malato Y, Gormond C, Willenbring H. Evidence against a stem cell origin of new hepatocytes in a common mouse model of chronic liver injury. Cell Rep. 2014;8(4):933–9.
7. Yanger K, Zong Y, Maggs LR, Shapira SN, Maddipati R, Aiello NM, Thung SN, Wells RG, Greenbaum LE, Stanger BZ. Robust cellular reprogramming occurs spontaneously during liver regeneration. Genes Dev. 2013;27(7):719–24.
8. Malato Y, Naqvi S, Schurmann N, Ng R, Wang B, Zape J, Kay MA, Grimm D, Willenbring H. Fate tracing of mature hepatocytes in mouse liver homeostasis and regeneration. J Clin Invest. 2011;121(12):4850–60.
9. Lu W-Y, Bird TG, Boulter L, Tsuchiya A, Cole AM, Hay T, Guest RV, Wojtacha D, Man TY, Mackinnon A, Ridgway RA, Kendall T, Williams MJ, Jamieson T, Raven A, Hay DC, Iredale JP, Clarke AR, Sansom OJ, Forbes SJ. Hepatic progenitor cells of biliary origin with liver repopulation capacity. Nature Cell Biol. 2015;17(8):971–83.
10. Huang MB, Chang A, Choi M, Zhou D, Anania FA, Shin CH. Antagonistic interaction between Wnt and Notch activity modulates the regenerative capacity of a zebrafish fibrotic liver model. Hepatology 2014;60(5):1753–66.
11. He J, Lu H, Zou Q, Luo L. Regeneration of liver after extreme hepatocyte loss occurs mainly via biliary transdifferentiation in zebrafish. Gastroenterology 2014;146(3):789–800.e8.
12. Choi TY, Ninov N, Stainier DY, Shin D. Extensive conversion of hepatic biliary epithelial cells to hepatocytes after near total loss of hepatocytes in zebrafish. Gastroenterology 2014;146(3):776–88.
13. Pisharath H, Rhee JM, Swanson MA, Leach SD, Parsons MJ. Targeted ablation of beta cells in the embryonic zebrafish pancreas using E. coli nitroreductase. Mech Dev. 2007;124(3):218–29.
14. Davison JM, Akitake CM, Goll MG, Rhee JM, Gosse N, Baier H, Halpern ME, Leach SD, Parsons MJ. Transactivation from Gal4-VP16 transgenic insertions for tissue-specific cell labeling and ablation in zebrafish. Dev Biol. 2007;304(2):811–24.
15. Curado S, Anderson RM, Jungblut B, Mumm J, Schroeter E, Stainier DYR. Conditional targeted cell ablation in zebrafish: A new tool for regeneration studies. Dev Dyn. 2007;236(4):1025–35.
16. Curado S, Stainier DYR, Anderson RM. Nitroreductase-mediated cell/tissue ablation in zebrafish: A spatially and temporally controlled ablation method with applications in developmental and regeneration studies. Nat Protoc. 2008;3(6):948–54.
17. Lowes KN, Brennan BA, Yeoh GC, Olynyk JK. Oval cell numbers in human chronic liver diseases are directly related to disease severity. Am J Pathol. 1999;154(2):537–41.

18. Stueck AE, Wanless IR. Hepatocyte buds derived from progenitor cells repopulate regions of parenchymal extinction in human cirrhosis. Hepatology 2015;61(5):1696–707.
19. Miyajima A, Tanaka M, Itoh T. Stem/progenitor cells in liver development, homeostasis, regeneration, and reprogramming. Cell Stem Cell 2014;14(5):561–74.
20. Curado S, Ober EA, Walsh S, Cortes-Hernandez P, Verkade H, Koehler CM, Stainier DYR. The mitochondrial import gene tomm22 is specifically required for hepatocyte survival and provides a liver regeneration model. Dis Model Mech. 2010;3(7–8):486–95.
21. Westerfield M. The zebrafish book. A guide for the laboratory use of zebrafish (Danio rerio), 5th ed. Eugene (OR): University of Oregon Press; 2007.
22. Ninov N, Borius M, Stainier DYR. Different levels of Notch signaling regulate quiescence, renewal and differentiation in pancreatic endocrine progenitors. Development 2012;139(9):1557–67.
23. Mosimann C, Kaufman CK, Li P, Pugach EK, Tamplin OJ, Zon LI. Ubiquitous transgene expression and Cre-based recombination driven by the ubiquitin promoter in zebrafish. Development 2011;138(1):169–77.
24. Ninov N, Hesselson D, Gut P, Zhou A, Fidelin K, Stainier DYR. Metabolic regulation of cellular plasticity in the pancreas. Curr Biol. 2013;23(13):1242–50.
25. Ko S, Choi TY, Russell JO, So J, Monga SPS, Shin D. Bromodomain and extraterminal (BET) proteins regulate biliary-driven liver regeneration. J Hepatol. 2016;64(2):3 16–25.
26. Shimizu N, Kawakami K, Ishitani T. Visualization and exploration of Tcf/Lef function using a highly responsive Wnt/beta-catenin signaling-reporter transgenic zebrafish. Dev Biol. 2012;370(1):71–85.
27. Ellett F, Pase L, Hayman JW, Andrianopoulos A, Lieschke GJ. mpeg1 promoter transgenes direct macrophage-lineage expression in zebrafish. Blood 2011;117(4):E49–E56.
28. Her GM, Chiang CC, Chen WY, Wu JL. In vivo studies of liver-type fatty acid binding protein (L-FABP) gene expression in liver of transgenic zebrafish (Danio rerio). FEBS Lett. 2003;538(1–3):125–33.
29. Harvie EA, Green JM, Neely MN, Huttenlocher A. Innate immune response to Streptococcus iniae infection in zebrafish larvae. Infect Immun. 2013;81(1):110–21.
30. Alexander J, Stainier DY, Yelon D. Screening mosaic F1 females for mutations affecting zebrafish heart induction and patterning. Dev Genet. 1998;22(3):288–99.
31. Dong PDS, Munson Ca, Norton W, Crosnier C, Pan X, Gong Z, Neumann CJ, Stainier DYR. Fgf10 regulates hepatopancreatic ductal system patterning and differentiation. Nat Genet. 2007;39(3):397–402.
32. Field HA, Ober EA, Roeser T, Stainier DY. Formation of the digestive system in zebrafish. I. Liver morphogenesis. Dev Biol. 2003;253(2):279–90.
33. Lorent K, Moore JC, Siekmann AF, Lawson N, Pack M. Reiterative use of the notch signal during zebrafish intrahepatic biliary development. Dev Dyn. 2010;239(3):855–64.
34. Kodama Y, Hijikata M, Kageyama R, Shimotohno K, Chiba T. The role of notch signaling in the development of intrahepatic bile ducts. Gastroenterology 2004;127(6): 1775–86.
35. Zong Y, Panikkar A, Xu J, Antoniou A, Raynaud P, Lemaigre F, Stanger BZ. Notch signaling controls liver development by regulating biliary differentiation. Development 2009; 136(10):1727–39.
36. Yang SL, Aw SS, Chang CQ, Korzh S, Korzh V, Peng JR. Depletion of Bhmt elevates sonic hedgehog transcript level and increases beta-cell number in zebrafish. Endocrinology 2011;152(12):4706–17.
37. Nejak-Bowen KN, Monga SPS. Beta-catenin signaling, liver regeneration and hepatocellular cancer: Sorting the good from the bad. Semin Cancer Biol. 2011;21(1):44–58.
38. Huang S-Ma, Mishina YM, Liu S, Cheung A, Stegmeier F, Michaud Ga, Charlat O, Wiellette E, Zhang Y, Wiessner S, Hild M, Shi X, Wilson CJ, Mickanin C, Myer V, Fazal A, Tomlinson R, Serluca F, Shao W, Cheng H, Shultz M, Rau C, Schirle M, Schlegl J, Ghidelli S, Fawell S, Lu C, Curtis D, Kirschner MW, Lengauer C, Finan PM, Tallarico JA, Bouwmeester T, Porter JA, Bauer A, Cong F. Tankyrase inhibition stabilizes axin and antagonizes Wnt signalling. Nature 2009;461(7264):614–20.
39. Sugiyama M, Sakaue-Sawano A, Iimura T, Fukami K, Kitaguchi T, Kawakami K, Okamoto H, Higashijima SI, Miyawaki A. Illuminating cell-cycle progression in the developing zebrafish embryo. Proc Natl Acad Sci USA 2009;106(49):20812–7.
40. Bird TGT, Lu WW-Y, Boulter L, Gordon-Keylock S, Ridgway Ra, Williams MJ, Taube J, Thomas Ja, Wojtacha D, Gambardella A and others. Bone marrow injection stimulates hepatic ductular reactions in the absence of injury via macrophage-mediated TWEAK signaling. Proc Natl Acad Sci USA 2013;110(16):6542–7.
41. Boulter L, Govaere O, Bird TG, Radulescu S, Ramachandran P, Pellicoro A, Ridgway RA, Seo SS, Spee B, Van Rooijen N and others. Macrophage-derived Wnt opposes Notch signaling to specify hepatic progenitor cell fate in chronic liver disease. Nat Med. 2012;18(4):572–9.
42. Lorent K, Gong W, Koo KA, Waisbourd-Zinman O, Karjoo S, Zhao X, Sealy I, Kettleborough RN, Stemple DL, Windsor PA, Whittaker SJ, Porter JR, Wells RG, Pack M. Identification of a plant isoflavonoid that causes biliary atresia. Sci Transl Med. 2015;7(286):286ra67.
43. Okabe H, Yang J, Sylakowski K, Yovchev M, Miyagawa Y, Nagarajan S, Chikina M, Thompson M, Oertel M, Baba H, Monga SP, Nejak-Bowen KN. Wnt signaling regulates hepatobiliary repair following cholestatic liver injury in mice. Hepatology 2016;64(5):1652–66.